

Spherical Vision Transformer for 360° Video Saliency Prediction

BMVC 2023 Submission # 317

Abstract

The growing interest in omnidirectional videos (ODVs) that capture the full field-of-view (FOV) has gained 360° saliency prediction importance in computer vision. However, predicting where humans look in 360° scenes presents unique challenges, including spherical distortion, high resolution, and limited labelled data. To address these challenges, we propose a novel vision-transformer-based model for omnidirectional videos named SalViT360 that leverages tangent image representations. We introduce a spherical geometry-aware spatio-temporal self-attention mechanism that is capable of effective omnidirectional video understanding. Furthermore, we present a consistency-based unsupervised regularization term for projection-based 360° dense-prediction models to reduce artefacts in the predictions that occur after inverse projection. Our approach is the first to employ tangent images for omnidirectional saliency prediction, and our experimental results on three ODV saliency datasets demonstrate its effectiveness compared to the state-of-the-art.

1 Introduction

As an important computer vision task, visual saliency prediction aims at predicting where people look in a scene. It is widely used in various areas, such as *saliency-guided* image and video compression [1, 2, 3, 4, 5], super-resolution [6, 7], and quality assessment [8, 9, 10, 11, 12] to exploit human perceptual features for enhancement. With the growing popularity of virtual reality (VR) applications and multimedia streaming, predicting saliency in 360° videos has received more attention recently. One primary challenge in processing 360° scenes is effectively representing omnidirectional data. Equirectangular Projection (ERP), where the full-FOV scene is projected on a 2D plane, is a common representation due to its computational simplicity. However, ERP suffers from spherical distortion, particularly towards the poles, which can significantly affect the geometric structure of the scene and degrade model performance. While previous works have proposed kernel transformations [13] and spherical convolutions [14, 15] to minimize this distortion on ERP, these methods come at the cost of computational complexity and the loss of global context in 360° scenes. Cubemap projection [16] is another common approach that addresses the distortion problem by approximately expressing the spherical scene with six faces of a cube. Although this approach eliminates the distortion to an extent, it breaks the continuity of neighbouring faces and introduces discrepancies in the predictions around the edges.

Previous works in 360° saliency prediction primarily focused on addressing this representation problem, with each method trying to balance representative power and computational complexity. Chao et al. [17] employed cubemap projection and fine-tuned the 2D

image saliency model SalGAN [13] on each cube face. Cheng et al. [19] extended cube-map projection with cube-padding to address the discontinuities on the face boundaries. Chao et al. [20] extended SalGAN360 with multi-view fusion. Dahou et al. [21] proposed a two-stream architecture to compute global and local saliency in omnidirectional videos. Their approach uses global prediction as a rough attention estimate, and the local stream on cube faces predicts local saliency. Zhang et al. [22] proposed spherical convolutions for saliency prediction. Qiao et al. [23] showed that the eye fixation distribution bias depends on the viewport locations, which motivated us to introduce *spherical position information* into our model. Yun et al [24] use local undistorted patches with deformable CNNs and use a ViT variant for self-attention across space and time. Djilali et al. [25] used a self-supervised pre-training based on learning the association between several different views of the same scene and trained a supervised decoder for 360° saliency prediction as a downstream task. Although their approach considers the global relationship between viewports, it ignores the temporal dimension that is crucial for video understanding.

The methods mentioned above share a common limitation in processing 360° data through projections or modified kernels and ignore the full field-of-view, which is critical for global scene understanding and saliency prediction. Thus, there is a need for an effective omnidirectional data processing method that minimizes spherical distortion while preserving the global context and avoiding computational overhead and artefacts introduced by the previous methods. Recently, Eder et al. [26] proposed tangent image representations, which use gnomonic projection to map a spherical image into multiple overlapping patches, where each patch is tangent to the faces of an icosahedron. This method tackles the problem of spherical distortion on the scene. However, to our interest, the dense-prediction models particularly suffer from discrepancies and artefacts on overlapping regions of tangent image patches after inverse projection to ERP. In this work, we propose using tangent images to process undistorted local viewports and develop a transformer-based model to learn their global association for saliency prediction in 360° videos. This is the first work that employs tangent images for omnidirectional saliency prediction, which is also capable of modelling the temporal dimension, motivated by the recent video transformer architectures, e.g., [27].

Proposed method and contributions: We use gnomonic projection to obtain multiple undistorted tangent images, which enables us to extract rich local spatial features using any pre-trained and fixed 2D backbone. Our extensive experiments demonstrate the effectiveness of our proposed SalViT360 model against the state-of-the-art on VR-EyeTracking [28], PVS-HMEM [29], and 360-AV-HM [30] datasets. Our contributions are three-fold:

- *Spherical geometry-aware spatial attention.* We aggregate global information on the sphere by computing self-attention among tangent viewports. We use tangent features as viewport tokens to address the quadratic complexity associated with spatial self-attention. We introduce 360° geometry awareness to the transformer by using learnable spherical position embeddings guided by per-pixel angular coordinates (ϕ, θ) , denoting *latitude* and *longitude* angles, respectively. The proposed position embedding method outperforms standard 1D embeddings, and it can easily be integrated into any transformer architecture designed for 360° images.
- *Viewport Spatio-Temporal Attention (VSTA).* The complexity of joint spatio-temporal self-attention increases quadratically with respect to the number of frames. With VSTA, we optimize this joint computation on tangent viewports from consecutive frames, where the spatio-temporal self-attention is performed in two stages: (1) Viewport Spatial Attention (VSA) and (2) Viewport Temporal Attention (VTA). In VSA,

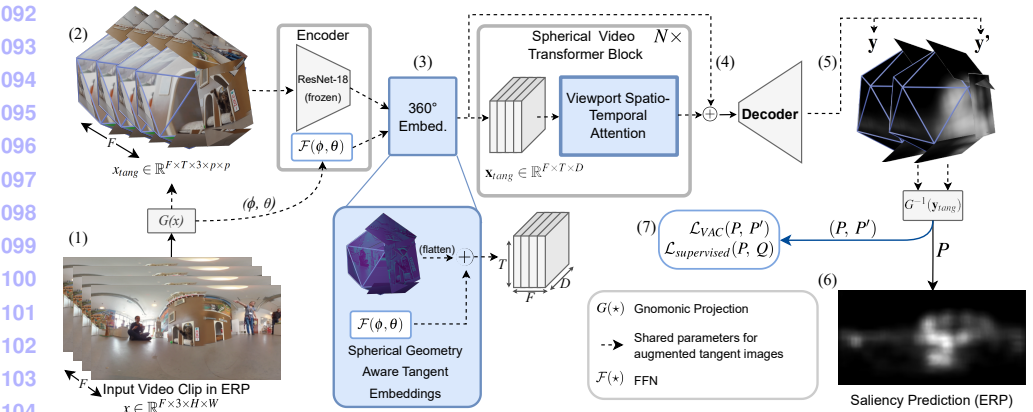


Figure 1: **Overview of the proposed SalViT360 model.** The ERP video clip of F frames (1) is projected to $F \times T$ tangent images per set (2). Each tangent image is encoded and fused with spherical-geometry-aware position embeddings (3) for the 360° video transformer to aggregate global information (4). The resulting features are decoded into saliency predictions in tangent space (5), which are projected back to ERP, giving the final saliency map (6). In addition to the supervised loss, the model is optionally trainable on $\mathcal{L}_{VAC}(P, P')$, which minimizes the difference between original (P) and augmented (P') tangent predictions (7). During test time, the model works with a single tangent set. For simplicity, only one set of tangent images is shown.

spherical geometry-aware self-attention is computed *intra-frame* level. The temporal information in the videos is encoded by a VTA, among tangent planes that point to the same direction in the *inter-frame* level.

- *Viewport Augmentation Consistency (VAC).* We propose an unsupervised, consistency-based loss for omnidirectional images, minimizing the discrepancies in overlapping regions of tangent predictions. The loss is computed between the weight-sharing saliency predictions of two tangent image sets which are generated with different configurations. This regularization method is suitable for any projection-based dense-prediction model. Importantly, VAC does not introduce any memory or time overhead during test time, as only one set of predictions is sufficient for inference.

2 Method

In Fig. 1, we present an overview of our proposed model SalViT360. We start with gnomonic projection [26] to obtain tangent images for each frame in the input video clip. These are passed to an encoder-transformer-decoder architecture. The image encoder extracts local features for each tangent viewport and reduces the input dimension for the subsequent self-attention stage. We map the pixel-wise angular coordinates to produce the proposed spherical geometry-aware position embeddings $\mathcal{F}(\phi, \theta)$ for the 360° transformer, enabling better learning of spatial representations. The transformer utilizes Viewport Spatio-Temporal At-

tention (VSTA) to capture inter and intra-frame global information across tangent viewports 138 in a temporal window. The transformed embeddings are then fed into a 2D CNN-based 139 decoder, which predicts saliency on the tangent images. We then apply inverse gnomonic 140 projection on the tangent predictions to obtain the final saliency maps in ERP. We propose 141 an unsupervised consistency-based Viewport Augmentation Consistency Loss to mitigate 142 the discrepancies after inverse gnomonic projection. The learnable parameters of the net- 143 work are in tangent space, allowing us to use large-scale pre-trained 2D models for feature 144 extraction, while the rest of the network is trained from scratch. 145

Gnomonic Projection and Encoder. We first project the input ERP clip $x \in \mathbb{R}^{F \times 3 \times H \times W}$ 146 to a set of tangent clips $x_{tang} \in \mathbb{R}^{F \times T \times 3 \times p \times p}$, where F , 3, H , and W are the number of 147 frames, channel dimension (RGB), height, and width of a given video, respectively. The 148 resulting tangent images have a patch size of $p \times p = 224 \times 224$ pixels. Number of tan- 149 gent images per frame T , and FOV are the projection hyperparameters which vary between 150 10/18 and $120^\circ/80^\circ$. We downsample and flatten the encoder features to obtain tangent 151 feature vectors with dimension $D = 512$. We map the angular coordinates (ϕ, θ) for each 152 pixel of the tangent viewports to the same feature dimension using an FC layer and sum 153 these embeddings with encoder features to obtain the proposed *spherical geometry-aware* 154 *embeddings* $\mathbf{x}_{tang} \in \mathbb{R}^{F \times T \times D}$ that are used in the transformer. 155

Viewport Spatio-Temporal Attention for 360° videos. While the pre-trained encoder extracts rich spatial features for each tangent image locally, aggregating the global context in the full-FOV is essential for 360° scene understanding. We propose a self-attention mechanism on tangent viewport features to achieve this. However, since incorporating the temporal dimension of the videos increases the number of tokens and thus the computational complexity, we approximate spatio-temporal attention with two stages: we apply temporal attention (1) among the same tangent viewports from consecutive F frames, then, spatial attention (2) among T tangent viewports in the same frame. This reduces the overall self-attention complexity from $F^2 \times T^2$ to $F^2 + T^2$. In this way, we effectively model the global context required for 360° video understanding. Fig. 2 illustrates our proposed *Viewport Spatio-Temporal Attention* for 360° videos.

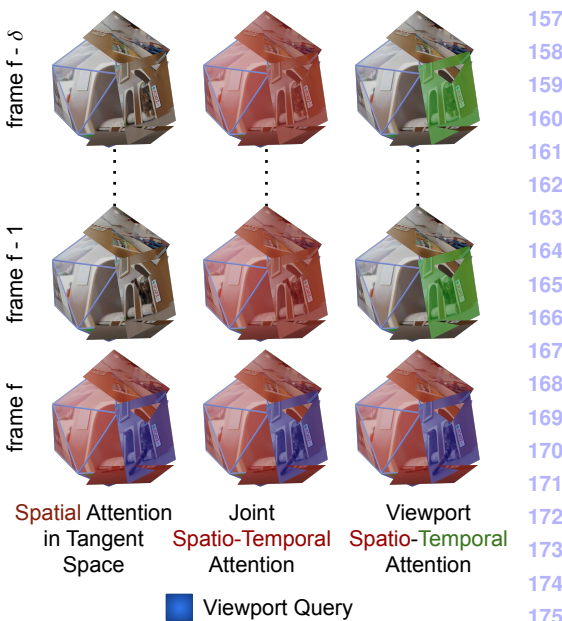


Figure 2: The proposed Viewport Spatio-Temporal Attention (VSTA) (right), as compared to Viewport Spatial Attention (VSA) (left) and Joint Spatio-Temporal Attention (middle). Red and Green viewports denote the self-attention neighborhood for each scheme. 177
178
179
180
181
182
183

184 **Decoder.** The decoder comprises four upsample layers followed by 3×3 convolutions and
 185 normalization layers. For a set of tangent clips, it takes the skip connection of encoder and
 186 transformer features $\mathbf{x}_{tang}^f \in \mathbb{R}^{T \times D \times 7 \times 7}$ of the last frame as input and outputs saliency prediction
 187 $\mathbf{y} \in \mathbb{R}^{T \times 56 \times 56}$ on tangent planes. The final ERP saliency maps are obtained by passing
 188 the tangent predictions to inverse gnomonic projection. We aggregate global information
 189 among tangent images through the transformer, however, each tangent plane is predicted
 190 separately in the decoder.

191 **Viewport Augmentation Consistency (VAC).** Our model effectively learns the overall saliency distribution with the supervised loss. However, since each tangent plane is predicted separately, the final ERP saliency map contains discrepancies in overlapping regions of tangent patches. To tackle this issue, we propose an unsupervised loss strategy, called *Viewport Augmentation Consistency* (VAC), for improving the consistency between the saliency predictions P and P' from two tangent projection sets. Specifically, we generate the second tangent set by applying different configurations, such as horizontally shifting the tangent planes on the sphere, using a larger FOV for the same viewports, and varying the number of tangent images at different viewports. We provide a detailed comparison of these approaches in the supplementary. VAC does not require any additional memory or time overhead since it uses the shared parameters of the whole model, and the forward pass is done in parallel. Furthermore, since the ERP predictions from the original P and augmented P' tangent sets are expected to be consistent, only one tangent set is sufficient for testing. The VAC loss is defined as:

$$\begin{aligned} \mathcal{L}_{VAC}(P, P') &= \mathcal{L}_{KLD}^{\text{weighted}}(P, P') + \mathcal{L}_{CC}^{\text{weighted}}(P, P'), \\ \mathcal{L}_{KLD}^{\text{weighted}}(P, P') &= \sum_{i,j} P_{i,j} \log \left(\epsilon + \frac{P_{i,j}}{P'_{i,j} + \epsilon} \right) \cdot w_{i,j}, \\ \mathcal{L}_{CC}^{\text{weighted}}(P, P') &= 1 - \frac{\sum (P \cdot P') \cdot w_{i,j}}{\sum (P \cdot P) \cdot \sum (P' \cdot P')} \end{aligned} \quad (1)$$

212 where P, P' are the saliency predictions from original and augmented viewports, and w is an optional weight matrix obtained from gnomonic projection to weigh the overlapping pixels of gnomonic projection on ERP predictions. Details for viewport augmentation approaches and the weighting operation are provided in the supplementary.

216

217

218 3 Experiments

219

220 3.1 Setup

221

222 **Datasets and pre-processing.** We use the publicly available *VR-EyeTracking* [28] dataset
 223 for training, which consists of 134 train and 74 test videos viewed by at least 31 subjects,
 224 lasting between 20 – 60 seconds. We sampled the videos at 16 fps with a resolution of
 225 960×1920 . For cross-dataset evaluation, we use the *PVS-HMEM* [29] and *360AV-HM* [30]
 226 datasets, which respectively contain 76 and 21 videos viewed by 58 and 15 subjects. The
 227 videos in the *PVS-HMEM* dataset have varying durations between 10 – 80 secs, while those
 228 in the *360AV-HM* dataset have a duration of 25 secs. The videos in both datasets have a
 229 frame rate between 24-60 fps.

Table 1: Performance analysis of SalViT360 against the state-of-the-art 360° saliency models on VR-EyeTracking, PVS-HMEM, 360AV-HM datasets. While the scores in **bold highlight the best performance, the underlined ones are the second best.**

Method	VR-EyeTracking				PVS-HMEM				360AV-HM			
	NSS↑	KLD↓	CC↑	SIM↑	NSS↑	KLD↓	CC↑	SIM↑	NSS↑	KLD↓	CC↑	SIM↑
CP-360	0.624	15.338	0.165	0.240	0.576	4.738	0.162	0.198	0.689	24.426	0.061	0.041
SalGAN360	1.753	10.845	0.370	0.355	1.513	4.394	0.314	0.291	0.719	25.301	0.065	0.036
MV-SalGAN360	1.818	8.713	0.382	0.357	1.546	4.112	0.316	0.295	0.716	25.322	0.066	0.036
ATSal	1.317	12.259	0.336	0.318	0.732	4.303	0.183	0.219	0.727	24.141	0.058	0.041
PAVER	1.511	13.267	0.307	0.294	0.750	3.736	0.224	0.269	0.732	23.944	0.065	0.035
Djilali et al.	3.183	<u>6.570</u>	<u>0.565</u>	0.475	<u>1.688</u>	<u>2.430</u>	<u>0.447</u>	0.404	<u>1.727</u>	<u>22.889</u>	0.148	0.085
SalViT360 (Ours)	<u>2.630</u>	5.744	0.586	0.492	2.191	1.841	0.626	0.495	1.946	22.711	0.168	0.093

Evaluation metrics and loss functions. We evaluate the performance of the models using the four most commonly used saliency evaluation metrics [31]: Normalized Scanpath Saliency (NSS), KL-Divergence (KLD), Correlation Coefficient (CC), and Similarity Metric (SIM). We use a weighted differentiable combination of KLD, CC, and Selective-MSE (MSE on normalized saliency maps at only eye-fixation points [52]) for the supervised loss, as given below:

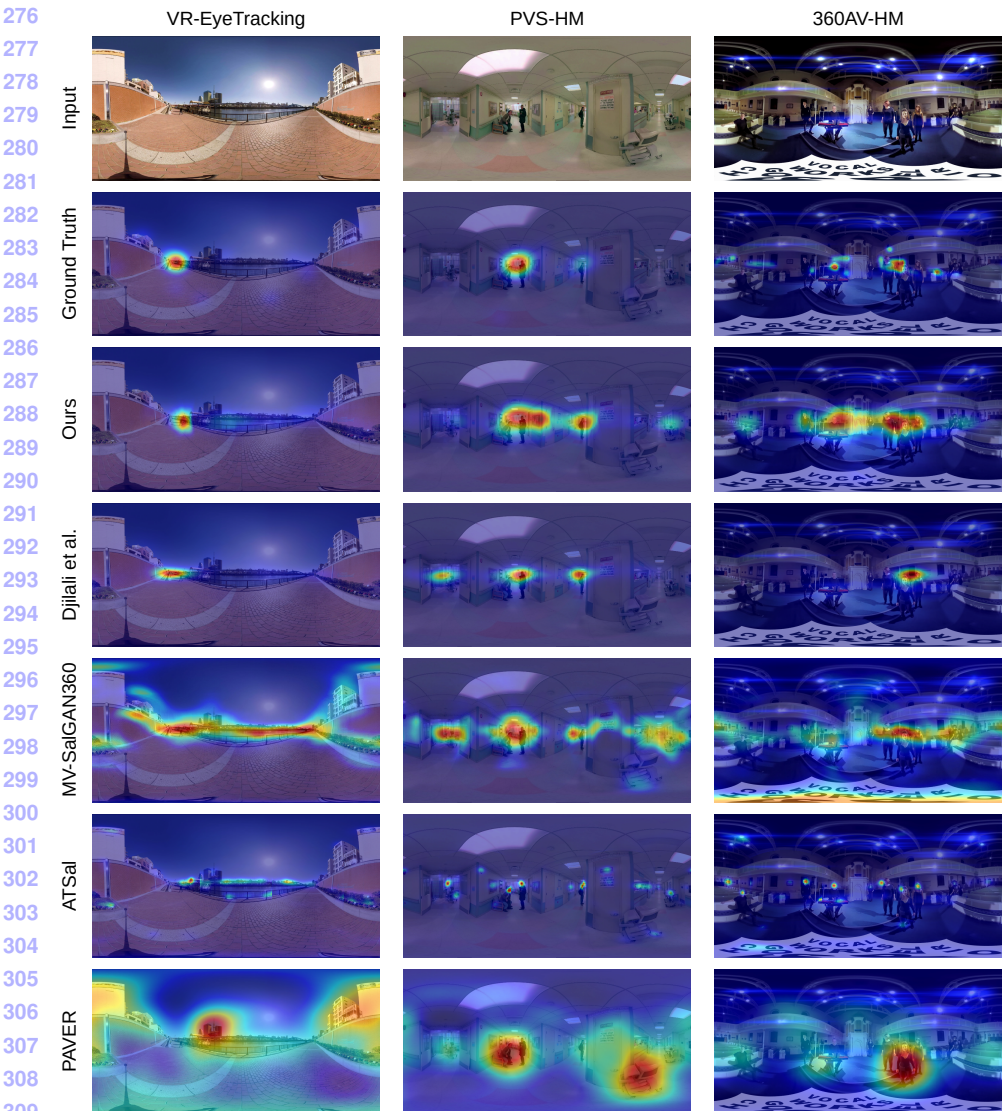
$$\mathcal{L}_{supervised}(P, Q_s, Q_f) = \mathcal{L}_{KLD}(P, Q_s) + \mathcal{L}_{CC}(P, Q_s) + \alpha \mathcal{L}_{SMSE}(P, Q_s, Q_f) \quad (2)$$

where P , Q_s , Q_f are the predicted saliency, ground truth density and fixation maps, respectively, and $\alpha = 0.005$.

Architecture and optimization details. We use a ResNet-18 encoder pre-trained on ImageNet and keep it frozen while extracting features. Our baseline 360° video transformer consists of 6 blocks with an embedding dimension of 512 and 8 attention heads. For the spatial position embeddings, we use linear projections of flattened pixel-wise angular coordinates, while we use rotary embeddings are used for the time dimension with a window size of $F = 8$. As in [77], we apply temporal self-attention followed by spatial self-attention in alternation. We train our SalViT360 model using the AdamW optimizer [33] with an initial learning rate of $1e-5$, default weight decay, and momentum parameters of $1e-2$ and $(\beta_1, \beta_2) = (0.9, 0.999)$, with a batch size of 16 for five epochs with early stopping.

3.2 Comparison with the State-of-the-art

In Table 1, we present the results of our SalViT360 model and the existing models. We evaluate the performance of SalViT360 with six state-of-the-art models for 360° image and video saliency prediction, namely CP-360 [32], SalGAN360 [33], MV-SalGAN360 [70], Djilali et al. [25], ATSal [21], PAVER [24]. ATSal, PAVER, and CP-360 are video saliency models; the rest are image-based models developed for the omnidirectional domain. On VR-EyeTracking test set, SalViT360 outperforms the state-of-the-art on three metrics and gives competitive results on NSS. On PVS-HMEM and 360-AVHM datasets, it outperforms the state-of-the-art by a margin on all metrics, demonstrating our proposed model’s cross-dataset performance. These results demonstrate that SalViT360 has a better generalization capability than the existing methods. The qualitative comparison in Fig. 3 also shows the effectiveness of our approach in highlighting the salient regions more accurately.



311 Figure 3: **Qualitative comparison on VR-EyeTracking [28], PVS-HM [29], and 360AV-
312 HM [30] datasets.** Our proposed approach gives better results compared to existing models.
313 The saliency predictions of our model better resemble the ground truth fixation density maps,
314 producing sparse estimates while covering the most dominant modes better.

3.3 Experimental Analysis and Ablation Studies

318 To assess the contribution of each component of our approach and to provide an in-depth
319 analysis of spatio-temporal modelling, we perform additional experiments on the test split of
320 VR-EyeTracking dataset and report our findings in Table 2 and Table 3. In these experiments,
321 we consider a baseline model comprised of a 2D ResNet-18 backbone, a vision transformer

Table 2: **Ablation study** for each component in our approach on the test split of the VR-322
EyeTracking dataset. 323

Method	# params	NSS↑	KLD↓	CC↑	SIM↑
VSA (w/ 1D Pos. Emb.)	30.28M	2.518	6.445	0.560	0.472
+ Spherical Pos. Emb.	30.78M	2.575	6.221	0.563	0.475
VSTA (w/ Sph. Pos. Emb.)	37.07M	2.664	6.174	0.570	0.479
+ VAC (w/o mask)	37.07M	2.624	6.011	0.576	0.490
+ VAC (w/ mask) [SalViT360]	37.07M	<u>2.630</u>	<u>5.744</u>	<u>0.586</u>	<u>0.492</u>
+ Late-Fusion	37.07M	2.578	4.654	0.592	0.495

with Viewport Spatial Attention, and a CNN-based decoder. 333

Spherical Position Embeddings. We compare the performance of our proposed *spherical* 335
geometry-aware spatial position embeddings with regular 1D learnable position embeddings. 336
The results on all four metrics show that our proposed embedding method outperforms it, 337
demonstrating that it is more suitable for processing spherical data with Vision Transformers. 338

Viewport Augmentation Consistency and Late-Fusion. We train our VSTA baseline using 339
only the supervised loss. We then compare this single-scale baseline to the one trained with 340
a weighted combination of the supervised loss ($\mathcal{L}_{supervised}$) and the consistency loss (\mathcal{L}_{VAC}). 341
Table 2 shows that VAC outperforms the VSTA baseline on three distribution-based saliency 342
evaluation metrics with a performance gain of 3.2% on KLD, 6.4% on CC, and 5.8% on 343
SIM, respectively. Lastly, we investigated the effect of using the predictions of two tangent 344
sets in the final prediction. We perform this with an optional late-fusion as element-wise 345
multiplication of two ERP predictions to highlight the consistently predicted salient regions 346
better. This simple optional fusion improves the performance on three metrics significantly, 347
with zero memory- and $0.5 \times$ time-overhead. We provide sample results for the qualitative 348
comparison of these components in Fig. 4, and detail them in the supplementary. 349

Spatio-Temporal modelling. We conducted several experiments to evaluate the effectiveness 351
of our proposed Viewport Spatio-Temporal Attention (VSTA) mechanism. In Table 2, 352
we compare Viewport Spatial Attention (VSA) and VSTA blocks to assess the contribution 353
of temporal information processing in omnidirectional videos. In Table 3, we compare our 354
VSTA with two distinct approaches, namely *2+1D-CNN* [34] backbone and *Offline EMA*. 355
2+1D-CNN backbone is an R2+1D model [35] which performs convolution over consecutive 356
frames, pre-trained on undistorted *normal-FOV* crops in 360° videos. We replace ResNet- 357
18 + VSTA with *2+1D-CNN* + VSA to introduce temporal features for spatial self-attention. 358
In the other setting, we keep ResNet-18 and VSA and apply a weighted exponential mov- 359

Table 3: **Spatio-temporal modelling performance** of SalViT360 compared against two 361
alternative approaches on the test split of the VR-EyeTracking dataset. 362

Method	# params	NSS↑	KLD↓	CC↑	SIM↑
VSA + <i>2+1D-CNN</i> Enc.	28.82M	2.568	5.915	0.568	0.477
VSA + <i>Offline EMA</i>	30.78M	2.591	6.018	0.566	0.477
SalViT360 (VSTA + VAC)	37.07M	2.630	5.744	0.586	0.492



Figure 4: **Qualitative comparison** for our *VSTA baseline* (third row), with the proposed *VAC loss* (fourth row), and the optional *late-fusion* (last row), compared to the ground truth.

ing average on F consecutive predictions for temporal aggregation. Additionally, we ablate on transformer depth, which shows that our VSTA blocks gradually learn better spatio-temporal representations in deeper layers. Our experiments demonstrate that the proposed VSTA mechanism outperforms the spatial-only setting and the other two spatio-temporal approaches. We refer the reader to the supplementary for comprehensive experiments on the effect of *the transformer depth*, and *temporal window size F* , along with the performance of *joint spatio-temporal attention*.

4 Conclusion

In this study, we proposed SalViT360, a transformer-based framework using tangent image representations for 360° video saliency prediction. We also introduced a spatio-temporal attention mechanism on tangent viewports to effectively capture the global and temporal context in omnidirectional videos. Our framework employs a new (model-agnostic) spherical geometry-aware position embedding structure based on angular coordinates. Lastly, we suggested an unsupervised, consistency-based loss function as a regularizer to the artefacts commonly observed in projection-based dense-prediction models. Our experimental results obtained from three omnidirectional video saliency datasets demonstrate that our proposed

SalViT360 model outperforms the state-of-the-art qualitatively and quantitatively. As a future research direction, we plan to investigate the impact of spatial audio in 360° videos and extend our proposal to the audio-visual domain.

References

- [1] Shengxi Li, Mai Xu, Yun Ren, and Zulin Wang. Closed-form optimization on saliency-guided image compression for hevc-msp. *IEEE Transactions on Multimedia*, 20(1):155–170, 2018.
- [2] Shiping Zhu and Ziyao Xu. Spatiotemporal visual saliency guided perceptual high efficiency video coding with neural network. *Neurocomputing*, 275:511–522, 2018.
- [3] Dipti Mishra, Satish Kumar Singh, Rajat Kumar Singh, and Divanshu Kedia. Multi-scale network (mssg-cnn) for joint image and saliency map learning-based compression. *Neurocomputing*, 460:95–105, 2021.
- [4] Shiping Zhu, Chang Liu, and Ziyao Xu. High-definition video compression system based on perception guidance of salient information of a convolutional neural network and hevc compression domain. *IEEE Transactions on Circuits and Systems for Video Technology*, 30(7):1946–1959, 2020.
- [5] Anjul Patney, Marco Salvi, Joohwan Kim, Anton Kaplanyan, Chris Wyman, Nir Benty, David Luebke, and Aaron Lefohn. Towards foveated rendering for gaze-tracked virtual reality. *ACM Trans. Graph. (TOG)*, 35(6):1–12, 2016.
- [6] Haoxiang Wang, Zhihui Li, Yang Li, Brij B Gupta, and Chang Choi. Visual saliency guided complex image retrieval. *Pattern Recognition Letters*, 130:64–72, 2020.
- [7] Zejiang Hou and Sun-Yuan Kung. Multi-dimensional dynamic model compression for efficient image super-resolution. In *Proceedings of the IEEE/CVF Winter Conference on Applications of Computer Vision*, pages 633–643, 2022.
- [8] Sheng Yang, Qiuping Jiang, Weisi Lin, and Yongtao Wang. Sgdnet: An end-to-end saliency-guided deep neural network for no-reference image quality assessment. In *Proceedings of the 27th ACM International Conference on Multimedia*, pages 1383–1391, 2019.
- [9] Mengmeng Zhu, Guanqun Hou, Xinjia Chen, Jiaxing Xie, Haixian Lu, and Jun Che. Saliency-guided transformer network combined with local embedding for no-reference image quality assessment. In *Proceedings of the IEEE/CVF International Conference on Computer Vision*, pages 1953–1962, 2021.
- [10] Jingwei Guan, Shuai Yi, Xingyu Zeng, Wai-Kuen Cham, and Xiaogang Wang. Visual importance and distortion guided deep image quality assessment framework. *IEEE Transactions on Multimedia*, 19(11):2505–2520, 2017.
- [11] Mai Xu, Chen Li, Zhenzhong Chen, Zulin Wang, and Zhenyu Guan. Assessing visual quality of omnidirectional videos. *IEEE Transactions on Circuits and Systems for Video Technology*, 29(12):3516–3530, 2019.

- 460 [12] Miaomiao Qiu and Feng Shao. Blind 360-degree image quality assessment via
461 saliency-guided convolution neural network. *Optik*, 240:166858, 2021.
- 462 [13] Yu-Chuan Su and Kristen Grauman. Learning spherical convolution for fast features
463 from 360 imagery. *Advances in Neural Information Processing Systems*, 30, 2017.
- 464
- 465 [14] Benjamin Coors, Alexandru Paul Condurache, and Andreas Geiger. Spherenet: Learn-
466 ing spherical representations for detection and classification in omnidirectional images.
467 In *Proceedings of the European conference on computer vision (ECCV)*, pages 518–
468 533, 2018.
- 469
- 470 [15] Carlos Esteves, Christine Allen-Blanchette, Ameesh Makadia, and Kostas Daniilidis.
471 Learning so (3) equivariant representations with spherical cnns. In *Proceedings of the*
472 *European Conference on Computer Vision (ECCV)*, pages 52–68, 2018.
- 473
- 474 [16] Ned Greene. Environment mapping and other applications of world projections. *IEEE*
475 *Computer Graphics and Applications*, 6(11):21–29, 1986.
- 476
- 477 [17] Fang-Yi Chao, Lu Zhang, Wassim Hamidouche, and Olivier Deforges. Salgan360:
478 Visual saliency prediction on 360 degree images with generative adversarial networks.
In *Proc. IEEE ICMEW*, 2018.
- 479
- 480 [18] Junting Pan, Cristian Canton, Kevin McGuinness, Noel E. O’Connor, Jordi Torres,
481 Elisa Sayrol, and Xavier and Giro-i Nieto. SalGAN: Visual saliency prediction with
482 generative adversarial networks. In *arXiv*, January 2017.
- 483
- 484 [19] Hsien-Tzu Cheng, Chun-Hung Chao, Jin-Dong Dong, Hao-Kai Wen, Tyng-Luh Liu,
485 and Min Sun. Cube padding for weakly-supervised saliency prediction in 360 videos.
In *Proc. IEEE/CVF CVPR*, pages 1420–1429, 2018.
- 486
- 487 [20] F. Chao, L. Zhang, W. Hamidouche, and O. Deforges. A multi-fov viewport-based
488 visual saliency model using adaptive weighting losses for 360-degree images. *IEEE*
489 *Transactions on Multimedia*, pages 1–1, 2020.
- 490
- 491 [21] Yasser Dahou, Marouane Tliba, Kevin McGuinness, and Noel O’Connor. ATSal: An
492 attention based architecture for saliency prediction in 360 videos. In *International*
493 *Conference on Pattern Recognition*, pages 305–320, 2021.
- 494
- 495 [22] Ziheng Zhang, Yanyu Xu, Jingyi Yu, and Shenghua Gao. Saliency detection in 360-
496 degree videos. In *Proc. ECCV*, September 2018.
- 497
- 498 [23] Minglang Qiao, Mai Xu, Zulin Wang, and Ali Borji. Viewport-dependent saliency
499 prediction in 360 video. *IEEE Trans. Multimed.*, 23:748–760, 2020.
- 500
- 501 [24] Heeseung Yun, Sehun Lee, and Gunhee Kim. Panoramic vision transformer for
502 saliency detection in 360-degree videos. In *Computer Vision–ECCV 2022: 17th Eu-
503 ropean Conference, Tel Aviv, Israel, October 23–27, 2022, Proceedings, Part XXXV*,
504 pages 422–439. Springer, 2022.
- 505
- 506 [25] Yasser Abdelaziz Dahou Djilali, Tarun Krishna, Kevin McGuinness, and Noel E.
507 O’Connor. Rethinking 360deg image visual attention modelling with unsupervised
508 learning. In *Proc. IEEE/CVF ICCV*, pages 15414–15424, October 2021.

-
- [26] Marc Eder, Mykhailo Shvets, John Lim, and Jan-Michael Frahm. Tangent images for mitigating spherical distortion. In *Proc. IEEE/CVF CVPR*, pages 12426–12434, 2020. 506
507
- [27] Gedas Bertasius, Heng Wang, and Lorenzo Torresani. Is space-time attention all you need for video understanding? In *Proceedings of the International Conference on Machine Learning (ICML)*, July 2021. 508
509
510
511
- [28] Yanyu Xu, Yanbing Dong, Junru Wu, Zhengzhong Sun, Zhiru Shi, Jingyi Yu, and Shenghua Gao. Gaze prediction in dynamic 360 immersive videos. In *Proc. IEEE/CVF CVPR*, pages 5333–5342, 2018. 512
513
514
- [29] Mai Xu, Yuhang Song, Jianyi Wang, MingLang Qiao, Liangyu Huo, and Zulin Wang. Predicting head movement in panoramic video: A deep reinforcement learning approach. *IEEE transactions on pattern analysis and machine intelligence*, 2018. 515
516
517
- [30] F. Y. Chao, C. Ozcinar, L. Zhang, W. Hamidouche, O. Deforges, and A. Smolic. Towards audio-visual saliency prediction for omnidirectional video with spatial audio. In *2020 IEEE International Conference on Visual Communications and Image Processing (VCIP)*, pages 355–358, 2020. 519
520
521
522
- [31] Zoya Bylinskii, Tilke Judd, Aude Oliva, Antonio Torralba, and Frédo Durand. What do different evaluation metrics tell us about saliency models? *IEEE Trans. Pattern Anal. Mach. Intell.*, 41(3):740–757, 2018. 523
524
525
526
- [32] Guanqun Ding, Nevrez İmamoğlu, Ali Caglayan, Masahiro Murakawa, and Ryosuke Nakamura. SalFBNet: Learning pseudo-saliency distribution via feedback convolutional networks. *Image and Vision Computing*, 120:104395, 2022. 527
528
529
- [33] Ilya Loshchilov and Frank Hutter. Decoupled weight decay regularization. *arXiv preprint arXiv:1711.05101*, 2017. 530
531
532
- [34] Pedro Morgado, Yi Li, and Nuno Vasconcelos. Learning representations from audio-visual spatial alignment. *Advances in Neural Information Processing Systems*, 33, 2020. 533
534
535
- [35] Du Tran, Heng Wang, Lorenzo Torresani, Jamie Ray, Yann LeCun, and Manohar Paluri. A closer look at spatiotemporal convolutions for action recognition. In *2018 IEEE/CVF Conference on Computer Vision and Pattern Recognition*, pages 6450–6459, 2018. 537
538
539
540
541
542
543
544
545
546
547
548
549
550
551